Physics Letters A 377 (2013) 2970–2978

Contents lists available at ScienceDirect

Physics Letters A

www.elsevier.com/locate/pla

Co-existing heat currents in opposite directions in graphene nanoribbons

Jingchao Zhang [a], Xinwei Wang [a,*], Huaqing Xie [b]

[a] Department of Mechanical Engineering, 2010 Black Engineering Building, Iowa State University, Ames, IA 50011, USA
[b] School of Urban Development and Environmental Engineering, Shanghai Second Polytechnic University, Shanghai 201209, PR China

ARTICLE INFO

Article history:
Received 17 July 2013
Received in revised form 4 September 2013
Accepted 6 September 2013
Available online 16 September 2013
Communicated by R. Wu

Keywords:
Graphene
Phonon transport
Co-existing heat currents
Weak mode-wide energy coupling

ABSTRACT

Using molecular dynamics simulations, we create an unprecedented scenario in graphene nanoribbons: co-existence of two heat currents in opposite directions at the same location. One heat current is carried by flexural mode phonons, and the other one by transverse/longitudinal modes phonons in the opposite direction. The local apparent thermal conductivity (κ_{app}) varies in a very large range: −468 to 1434 W/m K. The negative κ_{app} does not violate the second law of thermodynamics. It is a combined effect of the much higher thermal conductivity of flexural mode phonons and the weak coupling between them and transverse/longitudinal modes phonons.

1. Introduction

Graphene is a two-dimensional (2D) material that exhibits exceptional electric and optical properties [1,2]. The high electron mobility and thermal conductivity of graphene are of great interest for interconnects, electronic devices and radio frequency devices [3,4]. Similar to carbon allotropes like graphite and carbon nanotubes, graphene possesses high basal plane thermal conductivity due to its strong covalent bonding, light atomic weight and large crystalline domains [5]. Balandin et al. [6,7] reported extremely high thermal conductivity (κ) values in the range of 4840 ± 440 to 5300 ± 480 W/m K for mechanically exfoliated single layer graphene at room temperature (RT). Several groups have since measured the thermal conductivity of suspended graphene using different methods [4,8–10]. Their measured κ values range from 1800 W/m K to 5150 W/m K near RT. While for supported monolayer graphene, much lower κ values have been measured at ~600 W/m K at RT due to the flexural phonon coupling with the substrate [9,11]. The experimental work on the thermal conductivity of graphene stimulated extensive numerical work on this subject. Using classical molecular dynamics (MD) simulation, Hu et al. [12] calculated the thermal conductivity of symmetric graphene nanoribbons (GNRs) with dimension of 1.5×5.7 nm^2 to be around 2100 W/m K at 400 K. Evans et al. [13] reported a thermal conductivity at ~6000 W/m K for graphene sheet with dimensions of 10×10 nm^2 at 300 K. Other groups using equilibrium molecular dynamics (EMD) [14] and non-equilibrium molecular dynamics (NEMD) [15] came up with much lower thermal conductivities at 630 W/m K and 218 W/m K respectively for isolated graphene and armchair GNR at 300 K.

For a long time it has been tacitly accepted that the in-plane acoustic phonons are dominant in the thermal transport of graphene [16–19], recent studies have shown that the fact is quite different. Saito et al. [20] calculated the ballistic thermal conductance of graphene by investigating the dispersion relation of phonons and electrons. They demonstrated that the ballistic phonon conductance of graphene below about 20 K is mainly determined by the out-of-plane acoustic mode (ZA branch) and the in-plane acoustic modes (LA and TA branches) cannot be ignored above 20 K. By measuring the thermal transport of single layer graphene (SLG) supported on amorphous SiO_2, Seol et al. [11,21] performed a revised calculation and they showed that the ZA branch can contribute as much as 77% at 300 K and 86% at 100 K of the calculated thermal conductivity for suspended graphene due to the high specific heat and long mean scattering time of ZA phonons. Based on the exact numerical solution of the linear Boltzmann transport equation, Lindsay et al. [22,23] calculated the lattice thermal conductivity (κ_L) of graphene at 300 K and it turned out that the dominant contribution to κ_L comes from the ZA branch, which is greater than the combined TA and LA contributions. A symmetry-based selection rule and the anomalously large density of states of flexural phonons are used to explain their results. This unique feature in graphene's thermal conductivity gives rise to many peculiar properties of its thermal transport.

* Corresponding author. Tel.: +1 515 294 2085; fax: +1 515 294 3261.
E-mail address: xwang3@iastate.edu (X. Wang).

0375-9601/$ – see front matter
http://dx.doi.org/10.1016/j.physleta.2013.09.016

Our previous study revealed the fact that in a GNR system, the ZA branch has much higher thermal conductivity than the LA and TA branches [24,25]. Also, ZA ↔ ZA energy transfer is much faster than the ZA ↔ LA/TA phonon energy transfer. Using MD simulations, we have shown that under the influence of a moving or static localized heat source, the flexural mode (FM) phonons dissipate heat much faster than the longitudinal mode (LM) and transverse mode (TM) phonons, which gives rise to an energy inversion phenomenon at the system level [26]. Besides, due to the high thermal conductivity of flexural mode (ZM) phonons in GNRs, energy separation is observed between the in-plane and out-of-plane phonon modes after a steady state heat flux (q'') is imposed on the system. Such energy separation can hold for about 50 nm from the heating region.

The differential form of Fourier's law of heat conduction is expressed as $q'' = -\kappa \cdot \nabla T$, where q'' is the local heat flux, κ the material's thermal conductivity and ∇T the temperature gradient. The minus sign indicates the heat current flows from higher temperature regions to lower ones. For bulk materials, κ is size independent and only determined by the material's composition and structure. While for micro/nanoscale materials, κ is also affected by parameters like dimension and boundary condition. Non-Fourier thermal transport in micro/nanoscale materials has been studied extensively by previous research [27,28]. Generally, in order to define the local temperature, mode-wide thermal equilibrium among different phonon modes should be reached. However, since the thermal conductivities of different phonon modes in graphene have huge differences, it is possible that there is mode-wide energy difference during steady state heat conduction in graphene. In such scenario, the definition of temperature is no longer accurate to describe graphene's local energy level. And strictly speaking, thermal conductivity is also not well defined. Therefore, a nominal temperature (E_T) with unit K and apparent thermal conductivity (κ_{app}) with unit W/m K are brought up to give a better description.

In this work, phonon thermal transport in GNRs is investigated by using MD simulation. A peculiar heating and cooling technique is developed to induce mode-wide energy difference during steady state heat conduction. The unique thermal properties of GNR enable it to support a bi-directional heat transfer in the system. And when the bi-directional heat conduction reaches steady state, a single thermal conductivity cannot be used to reflect the relation between the heat flux and the temperature gradient. The calculated thermal conductivities are dependent on the net heat fluxes and the κ_{app} of graphene are calculated at positive, negative, zero and infinite values, depending on the proportions of each phonon mode energy added/subtracted to/from the heating/cooling areas.

2. Basis of physical problem and modeling

The second generation of Brenner potential [29]: reactive empirical bond-order (REBO), based on the Tersoff potential [30,31] with interactions between C–C bonds is applied in our MD simulation. In this work, the GNR systems have zigzag boundaries in the width direction and armchair boundaries in the length direction. Definitions of the zigzag and armchair boundaries can be literally understood and are depicted in Fig. 1(c). The edge carbon atoms are not hydrogen-passivated. Atomic configuration of the GNR system is shown in Fig. 1. The outermost layer of carbon atoms at each end (denoted in black) are fixed to avoid the spurious global rotation of the GNRs in the simulation [32]. Free boundary conditions are applied to the x and z directions. To compare the energy evolution of different phonon modes and the whole system, a nominal temperature E_i defined as $E_{k,i}/(1/2)k_B$ with unit K is used to represent the energy values in each phonon mode and a value E_T defined as $E_{k,T}/(3/2)k_B$ with unit K stands for the system's total energy. Here $E_{k,i}$ is the kinetic energy of carbon atoms for phonon mode i ($i = TM$, LM, or FM); $E_{k,T}$ is the total kinetic energy of carbon atoms and k_B is the Boltzmann constant.

Within the linear response regime, one would expect from Fourier's law of heat conduction that q'' changes proportionally with ∇T. However, in many low dimensional systems [33–37], it is found that q'' decreases with an increasing temperature bias (ΔT), which is known as negative differential thermal conductance (NDTC). Recent study by Hu et al. [33] revealed a tunable NDTC in rectangular and triangular GNRs, which results from the competition between decreasing κ and increasing ΔT beyond linear response regime. They demonstrated that the NDTC in GNR is caused by its temperature dependent thermal conductivity. However, it is worth noting that the thermal conductivity of GNR is not only temperature dependent, but also deviates much among in-plane and out-of-plane directions [11,20,22,24]. Therefore, it is of great interest to explore the peculiar thermal properties brought up by the thermal conductivity deviations among different phonon modes. Inspired by the strong mode-wide difference in sustaining thermal transport in GNR, bi-directional heat transfer in a rectangular GNR is explored in this work (as shown in Fig. 1). Four layers of carbon atoms at each end of the GNR system is grouped to add/subtract kinetic energy to/from the out-of-plane phonon mode (E_{FM}) and in-plane phonon modes (E_{LM} and E_{TM}) respectively. In traditional non-equilibrium molecular dynamic methods for thermal conductivity calculation, the hot and cold regions are created in the simulation domain by adding kinetic energy ΔE_k in the hot region and removing the same amount from the cold one while preserving linear momentum at each time step. The velocity of each atom is rescaled by the same factor χ. In this work, we use a modified velocity rescaling method to control the energy variation for each phonon mode, i.e., instead of adding/subtracting kinetic energy to all phonon modes, we manage to add kinetic energy only to the specified phonon mode and subtract kinetic energy from the others in the same region. Specifically, by adding kinetic energy to E_{FM} while subtracting kinetic energy from E_{LM} and E_{TM} at the left end of GNR and doing the opposite at the right end, a bi-directional heat conduction phenomenon is observed. This physical process is demonstrated in Figs. 1(a), (b) and (c). The local nominal temperature along the GNR is calculated from the kinetic energy of the three phonon modes averaged for 50 ps.

In this work, the phonon–phonon couplings among different phonon modes are considered in the graphene system naturally since the MD simulation tracks the full movement of each atom and the inter-atomic interaction. In our previous study [26], it has been demonstrated that the energy coupling between TM and LM phonons is much faster than that between TM/LM and FM phonons. At temperature ∼80 K, it is calculated that the phonon relaxation time between FM and TM/LM is 4.7 times larger than that between TM and LM, meaning the energy transfer between TM/LM and FM is much slower than that between TM and LM. Also, it is concluded that the energy coupling between FM and TM/LM phonons is not constant against their energy level: the coupling becomes stronger when the phonon energy is higher.

3. Results and discussion

3.1. Negative apparent thermal conductivity in GNR

A GNR with dimensions of 2.0×50.1 nm^2 ($x \times y$) is built. After 400 ps canonical ensemble (NVT) and 150 ps microcanonical ensemble (NVE) calculations, the system reaches thermal equilibrium at temperature 50 K. In our previous studies on GNR's thermal conductivity, we showed that quantum correction is of great importance to graphene's temperature and thermal conductivity calculations [24]. The MD temperature 50 K we used in this work corresponds to ∼300 K after quantum correction, which is

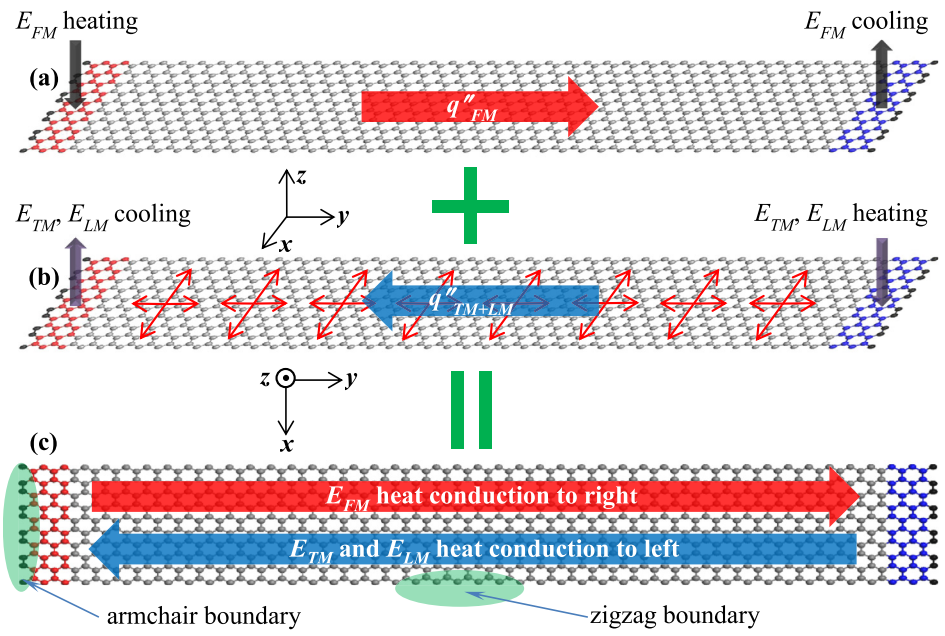

Fig. 1. Atomic configuration for studying the bi-directional heat conduction in graphene nanoribbons. The outermost layer of carbon atoms at each end (denoted in black) are fixed in position. (a) Kinetic energy is added to the FM phonons on the left side (red region) and subtracted from the right side (blue region). Heat current q''_{FM} is carried by FM phonons from left to right. (b) The in-plane longitudinal and transverse phonons are heated and cooled on the right and left sides respectively. Heat current q''_{TM+FM} is carried by TM/LM phonons from right to left. (c) By doing (a) and (b) simultaneously, a peculiar bi-directional heat conduction phenomenon in GNR is created. (For interpretation of the references to color in this figure legend, the reader is referred to the web version of this Letter.)

the room temperature in a lot of experimental work. If the system temperature changes substantially, the energy coupling rates between in-plane and out-of-plane phonon modes will also change. Details about this energy coupling change against temperature were reported in our previous work [26]. For FM phonons, kinetic energy $\Delta\dot{E}_{k,FM} = 2.17 \times 10^{-8}$ W is added to the left end and subtracted from the right end of the GNR constantly for 400 ps, while $\Delta\dot{E}_{k,TM} + \Delta\dot{E}_{k,LM} = 1.96 \times 10^{-8}$ W ($\Delta\dot{E}_{k,TM} = \Delta\dot{E}_{k,LM}$) is subtracted from the left TM + LM phonons and added to the right end TM + LM phonons of the GNR respectively for the same time span. A parameter μ defined as $\Delta\dot{E}_{k,FM}/(\Delta\dot{E}_{k,TM} + \Delta\dot{E}_{k,LM})$ is used to represent the heating and cooling ratio between the out-of-plane and in-plane phonons. In this case, μ equals 1.11. For simplicity, the value $(\Delta\dot{E}_{k,TM} + \Delta\dot{E}_{k,LM}) = 1.96 \times 10^{-8}$ W ($\Delta\dot{E}_{k,TM} = \Delta\dot{E}_{k,LM}$) remains constant for all the heating and cooling cases reported in this work, and variations are made by changing $\Delta\dot{E}_{k,FM}$. Since the layer distance in graphite is 0.335 nm, we use this value as the thickness for single layer graphene for thermal conductivity evaluation [38,39]. The cross-sectional area (A_c) is calculated at 6.7×10^{-19} m^2. Therefore the heat flux in the length direction can be calculated from the equation $q'' = Q/A_c$, from which the net heat flux is calculated as 3.23×10^9 W/m^2. The time step is 0.5 fs for all graphene calculations. After 400 ps bi-directional heating and cooling process, the heat conduction reaches steady state. Then another 50 ps is calculated for data collection and average. Nominal temperature distributions along the GNR system are shown in Figs. 2(a), (b) and (c). Fig. 2(a) shows the E_T energy distributions along the GNR while Figs. 2(b) and (c) are for the in-plane E_{TM}/E_{LM} and out-of-plane E_{FM} phonons respectively.

First of all, we can see from Fig. 2(b) that E_{TM} and E_{LM} have a positive gradient, meaning heat flux is negative (from right to left) for these modes of phonon energy since the heat flux is driven by temperature/energy differentials. On the other hand, E_{FM} has a negative gradient, meaning its heat flux is going from left to right. This simultaneous bi-directional heat conduction is very unique, and demonstrates, for the first time, that graphene as a unique material can support two heat currents in opposite directions at the same time. The main mechanism behind this phenomenon is the weak energy coupling between E_{TM}/E_{LM} and E_{FM}, and the much higher thermal conductivity by FM phonons. Although the FM mode has an energy differential from the transverse and longitudinal modes, due to the very weak energy coupling between them, this energy differential can hold for a very long distance. Consequently, the heat current sustained by the FM phonons can be different from that sustained by the LM/TM phonons, in both magnitude and direction.

Since q''_{FM} (from left to right) is larger than q''_{TM+LM} (from right to left), the net heat flux of the system q''_{total} is calculated at 3.23×10^9 W/m^2 in the direction from left to right. Generally speaking, under such condition one would expect that the temperature decreasing direction is in the same direction as the total heat flux. However, we clearly see in Fig. 2(a) that the positive gradient of E_T is from right to left, which is in the opposite direction of the total heat flux. This surprising phenomenon is caused by the very different heat conduction capacity between FM and LM/TM phonons. Although q''_{FM} is larger in this case, since the FM phonon sustains a much higher thermal conductivity, the temperature/energy gradient of FM phonons is smaller. On the other hand, even q''_{LM+TM} is smaller, the low thermal conductivity sustained by LM + TM phonons requires a larger temperature/energy gradient to sustain this heat flux. Therefore, at the system level, we see the heat flux direction is opposite to the prediction based on the overall energy gradient. According to Fourier's heat conduction equation, the apparent thermal conductivity $\kappa_{1.11}$ is calculated at -90.5 W/m K by linear fitting the E_T profile. The concept of thermal conductivity at nano/sub-nanoscales is not the same as that in the macroscopic space. It is more accurate to regard it as an effective thermal conductivity which represents the thermal transport capability at microscopic scales. This concept has been widely used in previous studies at micro/nanoscales [27,28].

Here we would like to stress this negative apparent thermal conductivity does not violate the second law of thermodynamics, nor does it tell the thermal conductivity can be negative for graphene. As discussed above, for each phonon mode, the heat

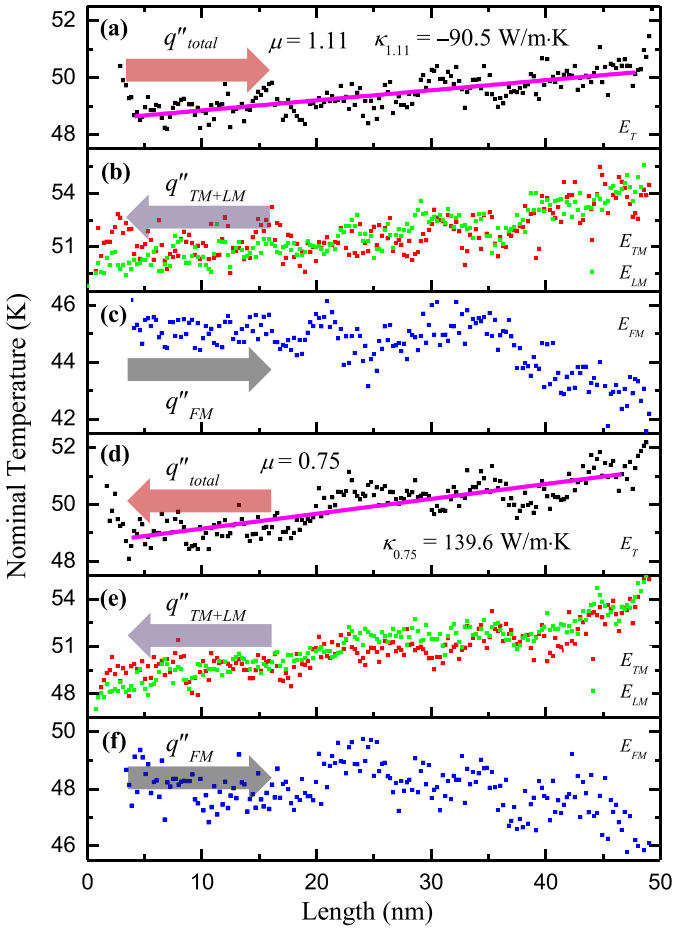

Fig. 2. Negative and positive κ_{app} calculations in the graphene system. (a), (b), (c) Nominal temperature distributions for $\mu = 1.11$. The E_T gradient and q''_{total} are in opposite directions, which indicates a negative κ_{app}. (d), (e), (f) Nominal temperature distributions for $\mu = 0.75$. In this case, q''_{total} is in the same direction as the E_T gradient and a positive κ_{app} is calculated.

current still flows from higher energy level to lower one, meaning its thermal conductivity is still positive. The negative apparent thermal conductivity originates from two factors: the very weak coupling between the FM and LM + TM phonons, and the much larger thermal conductivity sustained by FM phonons than that by LM + TM phonons. It tells one very important phenomenon in graphene: if there is phonon energy differential/separation between FM and LM + TM phonons during heat conduction, the local thermal conductivity based on Fourier's law of heat conduction will be different, depending on how much difference between the FM and LM + TM phonon energies, in both magnitude and gradient. The apparent thermal conductivity of graphene can be expressed as $\kappa_{app} = (\kappa_{TM} \cdot \partial E_{TM}/\partial y + \kappa_{LM} \cdot \partial E_{LM}/\partial y + \kappa_{FM} \cdot \partial E_{FM}/\partial y)/[(\partial E_{TM}/\partial y + \partial E_{LM}/\partial y + \partial E_{FM}/\partial y)/3]$. Only when the three phonon modes have the same temperature gradient in space, the thermal conductivity of graphene is the sum of the three modes thermal conductivities. Otherwise, the thermal conductivity of graphene will vary, depending on the extent of energy separation among phonon modes. More elaboration on this argument will be detailed in the following sections.

For comparison, another bi-directional heat conduction case with $\mu = 0.75$ is also calculated. All the calculation procedure and parameter settings are the same as the first case except for $\Delta \dot{E}_{k,FM} = 1.47 \times 10^{-8}$ W. The nominal temperature distributions of the system are shown in Figs. 2(d), (e) and (f). In this case, the net heat flux is calculated at -7.34×10^9 W/m^2 (from right to

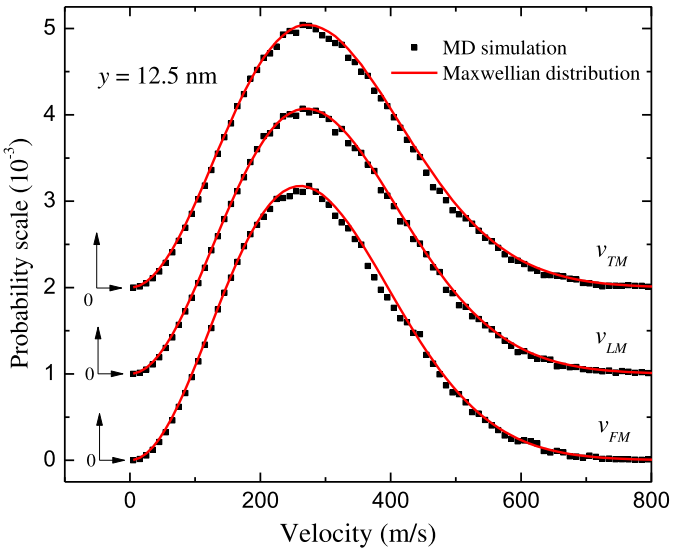

Fig. 3. Atomic velocity distributions for individual phonon mode in the 2.0×50.1 nm^2 GNR system at 12.5 nm region. Sound agreements between the MD simulation and Maxwellian velocity distributions are observed.

left), which is in the same direction as the negative gradient direction of E_T. The apparent thermal conductivity $\kappa_{0.75}$ is calculated at 139.6 W/m K. In the above two cases, both positive and negative κ_{app} are observed in the GNR system. In the following discussions, more bi-directional heat conduction cases with different μ values are calculated to explore the condition under which a negative κ_{app} will appear.

As mentioned in the above discussions, after 400 ps bi-directional heating and cooling process, the heat conduction in the 2.0×50.1 nm^2 GNR reaches steady state and the nominal temperature gradient for E_T becomes constant. However, since there are mode-wide energy differences between E_{FM} and E_{TM}/E_{LM}, energy exchange happens among different phonon modes. Therefore, it could be argued that the system has not yet reached thermal equilibrium in respect of individual phonon mode. To show that thermal equilibrium is established for both the GNR system and individual phonon branch, atomic velocity distribution at 12.5 nm, 25.0 nm and 37.5 nm locations in the length direction of the 2.0×50.1 nm^2 GNR is calculated for $\mu = 1.11$. At thermal equilibrium, the atomic velocity distribution should follow the Maxwellian distribution

$$P_M = 4\pi v^2 \left(\frac{m}{2\pi k_B T}\right)^{3/2} e^{-mv^2/2k_B T}, \tag{1}$$

where P_M is the probability for an atom moving with a velocity v. Since E_{TM}, E_{LM} and E_{FM} have different values within each region, the velocity distributions for each phonon mode are calculated. The v_{TM}, v_{LM} and v_{FM} distributions at 12.5 nm area are shown in Fig. 3, which indicates a good agreement between the velocity distribution and the Maxwellian distribution. Although mode-wide energy differences exist, each phonon mode has reached steady state heat conduction, which also shows the validity of temperature/energy use in the above calculations for each mode.

Error analysis is performed in our calculations. In this work, all the graphene systems reach thermal equilibrium after 400 ps canonical ensemble (NVT) and 100 ps microcanonical ensemble (NVE) calculations. In the thermal equilibrium calculations, the system temperature varies around the pre-set temperature 50.0 K. Take the $\mu = 0.75$ case as an example, after 500 ps thermal equilibrium calculation, the average temperature of the system is 50.1 K and the standard deviation (σ) of the system temperature variation is calculated at 1.2 K. Since the initial setup and

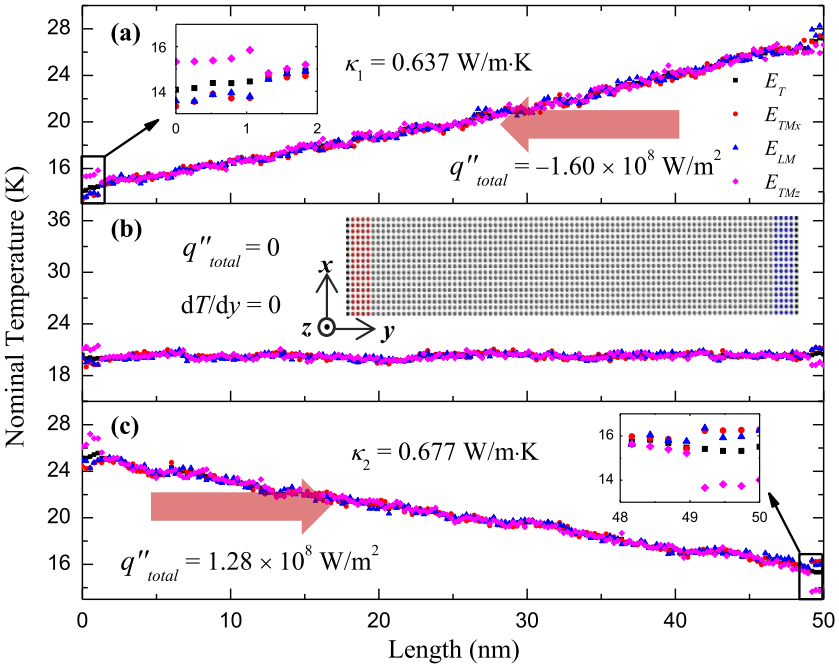

Fig. 4. Nominal temperature distributions under steady state bi-directional heat conduction in the solid argon system. (a) The net heat flux is 1.60×10^8 W/m^2 from right to left. The thermal conductivity κ_1 is calculated at 0.637 W/m K. The inset shows that the mode-wide energy separation only exists within the first 1 nm of the system and the bi-directional heat conduction does not penetrate deep to the system. (b) No temperature gradient is observed when the net heat flux is zero. Atomic structure of the solid argon system is shown in the inset. The outermost layer of argon atoms at each end (denoted in black) are fixed and free boundary conditions are applied to the x and z directions. Then four layers of argon atoms at each end (denoted in red and blue) are grouped to add/subtract energy. (c) The net heat flux is 1.28×10^8 W/m^2 from left to right and thermal conductivity κ_2 is calculated at 0.677 W/m K, which is consistent with κ_1. (For interpretation of the references to color in this figure legend, the reader is referred to the web version of this Letter.)

calculation processes are the same for all the systems, the error bar of temporal averaging will be around the same range, which is ± 1.2 K.

Also, it is worth noting that this peculiar heating and cooling method in the graphene system is created using MD simulations. This work is aimed at studying the unique thermal properties of graphene theoretically and pushing forward the science frontier. Therefore the results cannot be totally reproduced in the experimental studies. However, by using directional photon excitation with an electromagnetic field, it is possible to increase the thermal energy of graphene in certain phonon modes. For example, if the FM phonon energy is excited at one end of the graphene ribbon and TM/LM phonon energies are excited on the other end, a bi-directional heat transfer model will be created in the system, which is quite similar to the MD studies in this work.

3.2. Comparison study in solid argon system

Our interpretation of the negative κ_{app} observed in the GNR system is its much higher thermal conductivity by FM phonons, and weak energy coupling between the FM and LM/TM phonons. Therefore, for a normal material with the same thermal conductivity sustained by different phonon modes, the negative total temperature gradient should always be in the same direction as the net heat flux and its thermal conductivity should remain positive. To elaborate on this speculation, a solid argon system with dimensions of $4.3 \times 4.3 \times 50.1$ nm^3 ($x \times z \times y$) is used to investigate its κ_{app} under steady state bi-directional thermal conduction. Atomic configuration of the argon system is depicted in the inset of Fig. 4(b). The outermost layer of argon atoms at each end is fixed (denoted in black), and free boundary conditions are applied to the x and z directions. Four layers of argon atoms at each end of the system are grouped to add/subtract phonon energies. Since the nearest neighbor distance r_s in the fcc lattice of argon depends on the temperature, we use the expression given by Broughton and Gilmer [40] to initialize the r_s value, which is calculated at 3.768 Å at temperature 20 K. The interactions between argon atoms are described by the 12-6 LJ potential $\phi_{ij} = 4\varepsilon[(\sigma/r_{ij})^{12} - (\sigma/r_{ij})^6]$. The ε and σ are set as 0.01032 eV and 3.406 Å respectively and the cut off distance r_c is taken as 2.5σ. Time step is 5 fs for all calculations.

After 1 ns NVT and 500 ps NVE calculations, the argon system reaches thermal equilibrium at temperature 20 K. Then bi-directional heating and cooling process is performed for another 2 ns until the system reaches steady state heat conduction. Another 50 ps is calculated for the data collection and average. The nominal temperatures in the x, y and z directions are denoted as $E_{TM,x}$, E_{LM} and $E_{TM,z}$ respectively. Three different cases are calculated. Similarly, the $\Delta\dot{E}_{k,LM} + \Delta\dot{E}_{k,TMx}$ ($\Delta\dot{E}_{k,LM} = \Delta\dot{E}_{k,TMx}$) added/subtracted at each end is kept the same as 1.16×10^{-8} W for all cases, while $\Delta\dot{E}_{k,TMz}$ are set as 8.71×10^{-9} W, 1.16×10^{-8} W and 1.39×10^{-8} W. Their nominal temperature distributions are shown in Figs. 4(a), (b) and (c) respectively. Compared with the GNR cases above, it is observed in the solid argon system that the mode-wide energy differences only exist near the heating and cooling regions. The energy differences only exist in a very short distance (~ 1 nm) from the heating and cooling regions and the phonon energies then remain the same along the heat conduction direction, indicating strong phonon energy couplings among different phonon modes. Or we can say the bi-directional heat conduction only exists in very small regions close to the ends, then the heat conduction becomes one-directional. In Fig. 4(a), it is seen that the net heat flux q''_{total} and negative temperature gradient follows the same direction from right to left. And by linear fitting the E_T distribution, thermal conductivity κ_1 is calculated at 0.637 W/m K. No temperature gradient is observed in Fig. 4(b) when q''_{total} equals zero. Fig. 4(c) gives similar conclusions as Fig. 4(a) and the thermal conductivity κ_2 is calculated at 0.677 W/m K, which is consistent with κ_1. Previous studies reported thermal conductivity is around 1.4 W/m K for solid argon

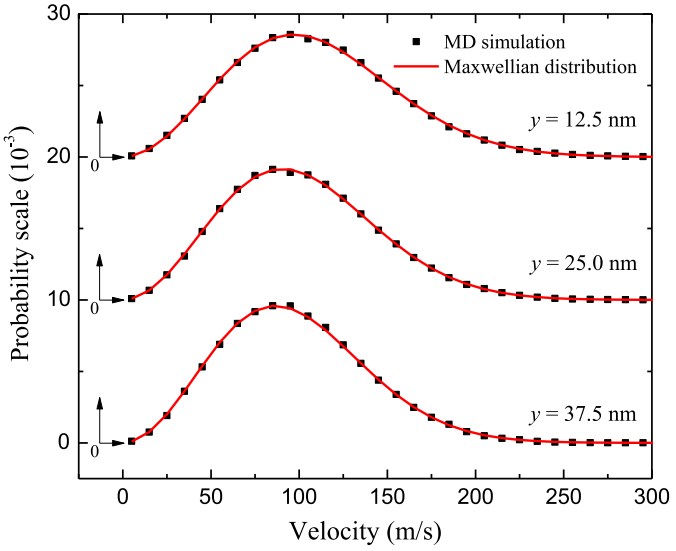

Fig. 5. Atomic velocity distributions under steady state bi-directional heat conduction in solid argon system. Different locations at 12.5 nm, 25.0 nm and 37.5 nm are used in the calculation and the MD results soundly match the Maxwellian distributions.

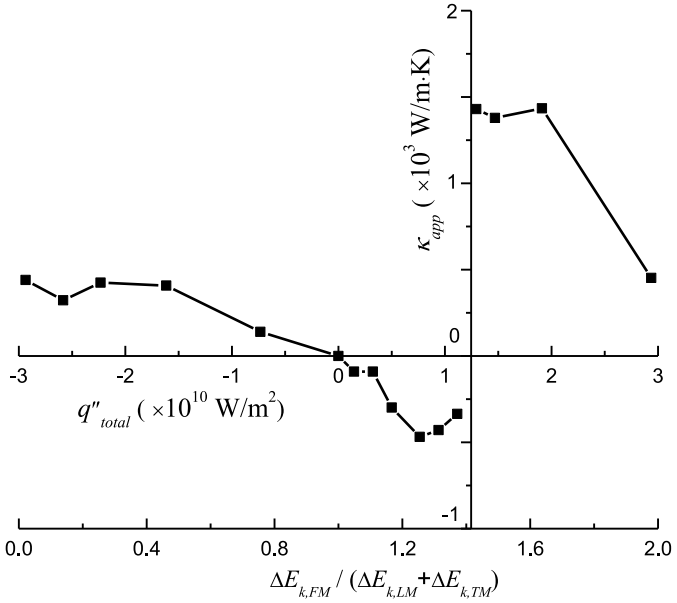

Fig. 6. Apparent thermal conductivity topology for the 2.0×50.1 nm^2 GNR system. The upper x-axis represents the net heat flux in the GNR system and the lower x-axis stand for the corresponding μ values. Negative κ_{app} is observed when μ is within the range 1.05–1.38.

at temperature 20 K [41–45]. Our calculated thermal conductivity for solid argon is lower than the experimental results. The small system size and the relative large surface/volume ratios contribute to the boundary phonon scattering during thermal conductance, which explains the slightly lower thermal conductivity calculated here for argon. Such effect has been confirmed by Zhong et al. [46] in their work, the thermal conductivity of a round argon wire of 4.3 nm diameter at 30 K was calculated to be 0.28 W/m K, much lower than the bulk value of 0.78 W/m K. Atomic velocity distribution in the solid argon system is also calculated and the results for the $\Delta \dot{E}_{k,TMz} = 1.39 \times 10^{-8}$ W case are shown in Fig. 5. Three different regions at 12.5 nm, 25.0 nm and 37.5 nm in the length direction are chosen. The MD results and the Maxwellian distributions have sound matches, indicating that the argon system has reached thermal equilibrium when the data are collected. Compared with the GNR cases, no mode-wide energy differences are observed under steady state heat conduction in the argon system except a very small (1 nm) region adjacent to the heating/cooling regions, and the thermal conductivity remains positive and consistent for all calculations. This further demonstrates the fact that the negative κ_{app} in GNR is caused by significant mode-wide deviation in thermal conductivity. To be specific, the FM phonon thermal conductivity is much higher than those of LM and TM phonons. The weak coupling between FM and LM/TM phonons is also an important factor that contributes to the negative κ_{app} in GNR.

3.3. κ_{app} topology for graphene

By applying bi-directional heat conduction in GNR, both positive and negative κ_{app} have been observed. To further explore this unique thermal transport phenomenon of graphene, cases with various $\Delta \dot{E}_{k,FM}$ values are calculated. Following the same calculation process and parameters in previous calculation, bi-directional heat conduction systems with μ values of 0, 0.12, 0.24, 0.45, 0.75, 1, 1.05, 1.11, 1.17, 1.26, 1.32, 1.38, 1.41, 1.44, 1.5, 1.65 and ∞ are calculated and their corresponding κ_{app} values are plotted in Fig. 6. The $\mu = \infty$ case means no $\Delta \dot{E}_{k,TM}$ or $\Delta \dot{E}_{k,LM}$ are added/subtracted to/from the GNR system and only $\Delta \dot{E}_{k,FM}$ is applied, while $\mu = 0$ means the opposite. Several very interesting phenomena are found in the κ_{app} calculations. First of all, when μ equals 1, which means the net heat flux q''_{total} is zero, a nominal temperature gradient with a value of 0.04 K/m is observed in the E_T distribution. Therefore, the κ_{app} of GNR has to be zero to satisfy the Fourier's heat conduction equation. And when μ equals 1.41, a net heat flux of value 1.2×10^{10} W/m^2 exists in the system. However, after the system reaches steady state, the nominal temperature gradient is calculated at 4.2×10^{-4} K/m, which is small enough to be considered zero. In such scenario, κ_{app} is calculated to be infinite according to Fourier's law of heat conduction. Based on our calculations, it is observed that when μ changes from 0 to 0.75, κ_{app} is positive. As μ becomes larger within the range of 1.05–1.38, κ_{app} is negative. Yet when μ changes from 1.44 to ∞, κ_{app} turns out positive again. It is concluded that κ_{app} of GNR is highly related with μ and the negative κ_{app} occurs only within a small range.

The physical meaning carried by the parameter μ indicates that when μ is smaller than 1, the bi-directional heat conduction in GNR is dominant by the in-plane LM and TM phonons, while when μ is larger than 1, the heat conduction is dominant by the out-of-plane FM phonons. It is observed that if the LM/TM phonon conduction is dominant, an overlap area among FM, LM and TM phonon energies exists at steady state. As μ increases, the overlap regions become smaller and when μ is larger than 1, no energy overlap is observed. To give a better description, nominal temperature distributions for μ values of 0.24, 0.75, 1.2 and 1.5 are shown in Fig. 7. The reasons for this phenomenon are the high thermal transport capacity of the FM phonons in GNR and the weak energy coupling between the FM and LM/TM phonons. Since the FM phonons have a much higher thermal conductivity in GNR, the thermal energies carried by the FM phonons will be transported to the heat sink much faster than those of LM and TM phonons. Therefore, if the same amount of thermal energy is added/subtracted to/from the FM and TM/LM phonons, the local E_{FM} values will eventually be smaller than the E_{LM}/E_{TM} along the heat conduction direction. Under this condition, the LM/TM phonons will keep transferring energy to the FM phonons as long as mode-wide energy differences exist. However, if the LM/TM phonon conduction is dominant in GNR ($\mu < 1$), the FM phonons will only be assigned with a small portion of the total heat conduction. The temperature/energy gradient of FM phonons will be very small. Therefore a smaller energy difference emerges between FM and

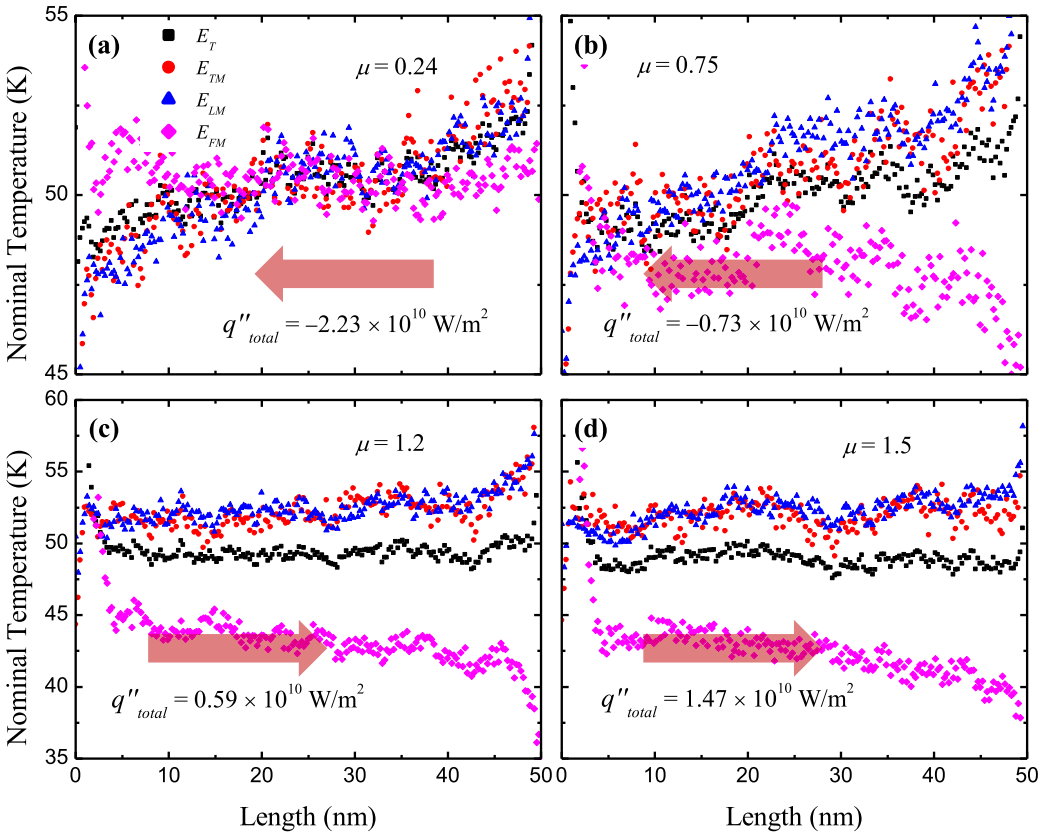

Fig. 7. Phonon energy evolutions for $\mu < 1$ and $\mu > 1$ cases. (a), (b) When the in-plane LM/TM phonon heat conduction is dominant ($\mu < 1$), an energy overlap is observed among different phonon modes. The length of the overlap region decreases with increasing μ. (c), (d) When the flexural phonon thermal transport is dominant ($\mu > 1$), there is no energy overlap among different phonon modes and the mode-wide energy separation increases with μ.

LM + TM phonons. This leads to an energy overlap among the three phonon mode, as is shown in Figs. 7(a) and (b). Figs. 7(c) and (d) demonstrate that when the FM phonon heat conduction is dominant ($\mu > 1$), the overlap will be suppressed. As the μ value increases, more heat will be carried by the FM phonons and the mode-wide energy differences will become larger and larger. This growing energy difference will enhance the energy transfer from E_{LM}/E_{TM} to E_{FM}, which leads to a smaller nominal temperature gradient for the E_{LM} and E_{TM}, as is shown in Figs. 7(c) and (d). It is worth noting that when energy overlap happens among the in-plane and out-of-plane phonons, the bi-directional heat conduction does not exist over the entire length and only exists in the energy separation regions. In other words, mode-wide energy separation is a necessary condition for the bi-directional heat conduction. Energy separation among phonon modes is a very important phenomenon in graphene, even under normal heat conduction conditions. More detailed analysis about energy separation, including the effect of temperature jump/drop from heating/cooling regions to the normal heat conduction region will be elaborated in our near-future publications since this work is focused on the bi-directional heat conduction and the apparent thermal conductivity (κ_{app}). In experimental studies, the value of μ can be changed by varying the ratios of in-plane and out-of-plane energies added to the graphene system.

3.4. Single-end bi-directional heat conduction and the length effect

To further explore the thermal behavior of graphene under bi-directional heat conduction, a single-end heating and cooling method is applied to the 2.0×50.1 nm^2 ($x \times y$) GNR system. This time, only the left end of the GNR is used to apply the FM phonon heating and LM/TM phonon cooling. The same method is also applied to a $4.3 \times 4.3 \times 50.1$ nm^3 ($x \times z \times y$) solid argon system for comparison. After the GNR system reaches thermal equilibrium at temperature 50 K, $\Delta \dot{E}_{k,FM}$ of value 1.96×10^{-8} W is added to the left end and $\Delta \dot{E}_{k,TM} + \Delta \dot{E}_{k,LM}$ ($\Delta \dot{E}_{k,TM} = \Delta \dot{E}_{k,LM}$) of the same value is subtracted from the same region for 400 ps. Another 50 ps is calculated for the data collection and average. The results are shown in Figs. 8(a), (b) and (c). The nominal temperature distributions show that the thermal energy is carried by the FM phonons from left to right and then carried back by the LM/TM phonons from right to left. Since the kinetic energy added/subtracted has the same amount at the left end, the net heat flux of the system is zero. However, a nominal temperature gradient 0.025 K/m is observed from the profile of E_T, which indicates that κ_{app} of graphene is zero. As for the solid argon system, after it reaches thermal equilibrium at temperature 20 K, bi-directional heating and cooling is applied on the left end for 2 ns and the thermal energy added/subtracted equals 1.16×10^{-8} W. The nominal temperature distributions are shown in Fig. 8(d). It is found that the nominal temperature gradient is zero, which satisfies the Fourier's heat conduction equation. For argon, only in a very small region (~1.0 nm) next to the left end that we found energy separation between $\Delta \dot{E}_{k,TMz}$ and $\Delta \dot{E}_{k,LM}/\Delta \dot{E}_{k,TMx}$, meaning the bi-directional heat conduction does not penetrate deep to the system.

The calculated high thermal conductivity values of graphene suggest that the mean free path in GNR is long even at room temperature. This may result in a strong length dependence of GNR's thermal conductivity. Therefore, the traditionally defined thermal conductivity is no longer an intrinsic property of GNR. Instead, it changes with the length. Thus it is necessary to explore the length effect on the bi-directional heat conduction of GNR and observe

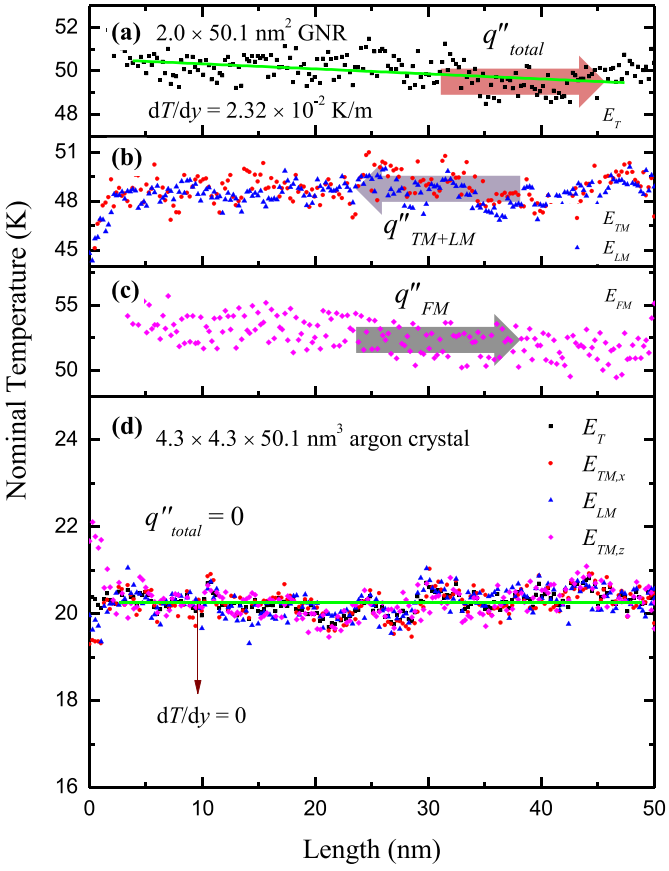

Fig. 8. Nominal temperature distributions for the bi-directional heat transfer in GNR and solid argon with one-end heating/cooling. The net heat flux equals zero for both cases. For the GNR system, the nominal temperature gradient equals 0.0232 K/m, which indicates a zero value κ_{app} according to Fourier's law of heat conduction. While for the solid argon system at temperature 20 K, the temperature gradient is calculated at zero.

the κ_{app} change with length. A 2.0×100.0 nm^2 $(x \times y)$ GNR is built to compare with the former 2.0×50.1 nm^2 case. When $\mu = 0.45$, κ_{app} of 100.0 nm GNR is calculated at 487 W/mK, which is 16% larger than that of 50.1 nm (408 W/mK). When $\mu = 1.14$, the calculated κ_{app} of 100.0 nm GNR is -605 W/mK, which is 34% larger than that of 50.1 nm (-451 W/mK). By comparing the results above, it is ready to conclude that the κ_{app} values of GNR will increase with length while preserving the signs.

To better analyze the thermal conductivity in the graphene system, mean free paths for individual phonon modes are calculated and the results are shown in Fig. 10. The phonon behavior in graphene can be well understood from its dispersion relations in the k-space. The dispersion relations are computed by taking the two-dimensional Fourier transform of atomic vibration in the space and the energy density in (ω, k) space is expressed as [47]:

$$\psi = \left| \frac{1}{N} \int v_\alpha \exp(iky - i\omega t)\, dt\, dy \right| \quad (\alpha = x, y, z), \tag{2}$$

where N is the number of atoms in the system and y is the heat conduction direction. The velocity vector is projected to the x, y and z directions to calculate the phonon energy density for transverse mode (TM), longitudinal mode (LM) and flexural mode (FM) phonons respectively. Similar method has been used to analyze individual phonon properties for various material systems [47–52]. It has been demonstrated that Eq. (2) is a linear superposition of Lorentzian functions with centers at phonon frequency ω_0 [50, 53]:

$$\psi = \frac{C}{\sqrt{[2\tau(\omega - \omega_0)]^2 + 1}}, \tag{3}$$

where C is the combination of coefficients in the Lorentzian function and τ is the phonon relaxation time. By fitting the phonon frequencies calculated from Eq. (2), the phonon relaxation time can be calculated for different k values. Differentiation is then performed on the dispersion relation profiles to find out corresponding phonon propagating speed v for each τ. It is worth noting that since k and ω are highly correlated in the reciprocal space, the phonon mean free path (l) can be directly calculated using the above method as ψ also centers at wave vector k_0 as $\psi = C_k/\sqrt{[2l(k-k_0)]^2 + 1}$. However, not all k values are available in the calculation of dispersion relation. The minimum increment of k depends on the size of the graphene system. Therefore, a large simulation domain is needed to achieve k grid with reasonable resolution, which dramatically increases the computation time. In this work, a time range of 10 ps is used in the calculation of graphene's dispersion relation, corresponding to a resolution of 0.2π THz in the ω-space. Since the thermal transport in graphene is dominant by acoustical phonon modes [4,6,14,36,46], only low frequency (0–20 THz) phonon spectrums are calculated. Dispersion relations for the 2.0×50.1 nm^2 GNR system are shown in Fig. 9. The calculated results have sound agreement with previous studies [54]. Phonon mean free paths are calculated accordingly and the results are shown in Fig. 10. It can be seen that the phonon mean free path is distributed within the range 0–150 nm, smaller than previous reported value (775 nm) [4] due to the confined dimension of graphene used in this study. Qiu et al. [55] also calculated the phonon mean free path of suspended GNR with dimensions of 4.4×4.3 nm^2 and their results are in the same range with those reported in our work.

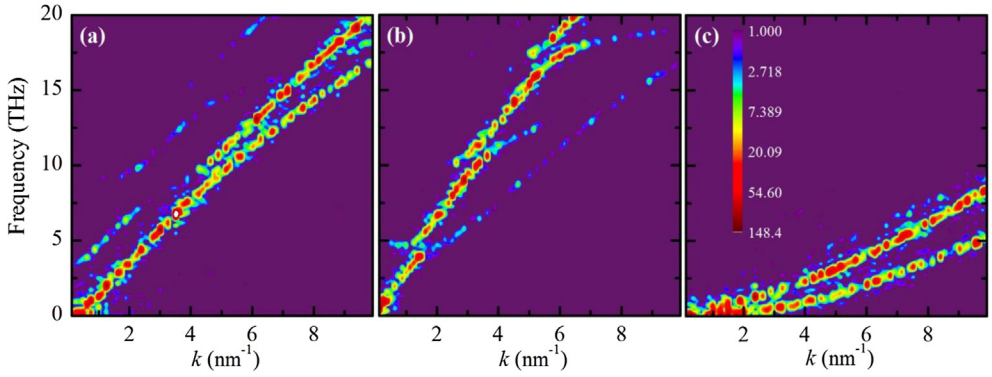

Fig. 9. Dispersion relations for the 2.0×50.1 nm^2 GNR system. (a), (b), (c) represent transverse, longitudinal and flexural phonon modes respectively.

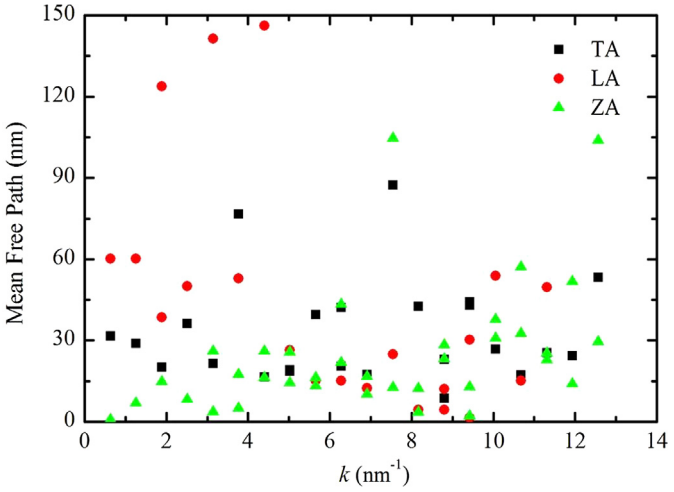

Fig. 10. Mean free path of TA, LA and ZA phonon modes in k-space.

4. Conclusion

In this work, phonon thermal transport in GNR was investigated under different FM and TM/LM phonon heating and cooling using MD simulation. A nominal temperature represented by the kinetic energy is used to evaluate the energy levels for each phonon mode. Due to the phonon mode energy deviations at the equilibrium state, the traditional thermal conductivity is not applicable. Instead, an apparent thermal conductivity (κ_{app}) is used in this work to represent the calculated κ from the Fourier's Law. Under such scenario, a negative apparent thermal conductivity is possible since the temperature gradient and the overall heat flux could be in opposite directions. It was observed that over a very long distance (up to 100 nm), unprecedented bi-directional heat currents emerged: FM and TM + LM phonons carried heat currents in opposite directions at the same time. The very weak energy coupling between FM and TM + LM phonons played a critical role in this bi-directional heat conduction. Both positive and negative κ_{app} were observed under steady state bi-directional heat conduction in GNR. The calculated negative κ_{app} does not violate the second law of thermodynamics because for each phonon mode, the heat current still flows from higher energy level to lower one, meaning its thermal conductivity is still positive. The negative κ_{app} originated from two factors: the very weak coupling between the FM and LM + TM phonons, and the much larger thermal conductivity sustained by FM phonons than that by LM + TM phonons. It was shown that thermal equilibrium was established for each phonon mode during steady state heat conduction. The mode-wide energy difference became greater when the heat current was dominated by FM phonons. The topology of κ_{app} for GNR was calculated with different μ values. When μ was within the range 1.05 to 1.38, κ_{app} was negative. Zero and infinite κ_{app} values were also observed during the steady state bi-directional heat transfer in GNR. The length effect on the bi-directional heat conduction was also explored and the results showed that if the length of the GNR increases, κ_{app} will also increase while its sign remains unchanged.

Acknowledgements

Support of this work by the Office of Naval Research (N000141210603), Army Research Office (W911NF-12-1-0272), and National Science Foundation (CBET-0931290, CBET-1235852) is gratefully acknowledged. H.X. thanks the great support from National Science Foundation of China (51176106). X.W. and H.X. also thank the support by the Eastern Scholar Program of Shanghai.

References

[1] R.R. Nair, P. Blake, A.N. Grigorenko, K.S. Novoselov, T.J. Booth, T. Stauber, N.M.R. Peres, A.K. Geim, Science 320 (2008) 1308.
[2] Y.B. Zhang, Y.W. Tan, H.L. Stormer, P. Kim, Nature 438 (2005) 201–204.
[3] M. Freitag, M. Steiner, Y. Martin, V. Perebeinos, Z.H. Chen, J.C. Tsang, P. Avouris, Nano Lett. 9 (2009) 1883–1888.
[4] S. Ghosh, I. Calizo, D. Teweldebrhan, E.P. Pokatilov, D.L. Nika, A.A. Balandin, W. Bao, F. Miao, C.N. Lau, Appl. Phys. Lett. 92 (2008) 151911.
[5] M.M. Sadeghi, M.T. Pettes, L. Shi, Solid State Commun. 152 (2012) 1321–1330.
[6] A.A. Balandin, S. Ghosh, W.Z. Bao, I. Calizo, D. Teweldebrhan, F. Miao, C.N. Lau, Nano Lett. 8 (2008) 902–907.
[7] A.A. Balandin, Nat. Mater. 10 (2011) 569–581.
[8] J.U. Lee, D. Yoon, H. Kim, S.W. Lee, H. Cheong, Phys. Rev. B 83 (2011) 081419.
[9] W.W. Cai, A.L. Moore, Y.W. Zhu, X.S. Li, S.S. Chen, L. Shi, R.S. Ruoff, Nano Lett. 10 (2010) 1645–1651.
[10] S.S. Chen, A.L. Moore, W.W. Cai, J.W. Suk, J.H. An, C. Mishra, C. Amos, C.W. Magnuson, J.Y. Kang, L. Shi, R.S. Ruoff, ACS Nano 5 (2011) 321–328.
[11] J.H. Seol, I. Jo, A.L. Moore, L. Lindsay, Z.H. Aitken, M.T. Pettes, X.S. Li, Z. Yao, R. Huang, D. Broido, N. Mingo, R.S. Ruoff, L. Shi, Science 328 (2010) 213–216.
[12] J.N. Hu, X.L. Ruan, Y.P. Chen, Nano Lett. 9 (2009) 2730–2735.
[13] W.J. Evans, L. Hu, P. Keblinski, Appl. Phys. Lett. 96 (2010) 203112.
[14] H.J. Zhang, G. Lee, A.F. Fonseca, T.L. Borders, K. Cho, J. Nanomater. 2010 (2010) 537657.
[15] Z.X. Guo, D. Zhang, X.G. Gong, Appl. Phys. Lett. 95 (2009) 163103.
[16] D.L. Nika, E.P. Pokatilov, A.S. Askerov, A.A. Balandin, Phys. Rev. B 79 (2009) 155413.
[17] D.L. Nika, S. Ghosh, E.P. Pokatilov, A.A. Balandin, Appl. Phys. Lett. 94 (2009) 203103.
[18] P.G. Klemens, Int. J. Thermophys. 22 (2001) 265–275.
[19] P.G. Klemens, J. Wide Bandgap Mater. 7 (2000) 332–339.
[20] K. Saito, J. Nakamura, A. Natori, Phys. Rev. B 76 (2007) 115409.
[21] R. Prasher, Science 328 (2010) 185–186.
[22] L. Lindsay, D.A. Broido, N. Mingo, Phys. Rev. B 82 (2010) 115427.
[23] L. Lindsay, D.A. Broido, N. Mingo, Phys. Rev. B 83 (2011) 235428.
[24] J.C. Zhang, X.P. Huang, Y.N. Yue, J.M. Wang, X.W. Wang, Phys. Rev. B 84 (2011) 235416.
[25] J.C. Zhang, X.W. Wang, Nanoscale 5 (2013) 734–743.
[26] J. Zhang, X. Wang, H. Xie, Phys. Lett. A 377 (2013) 721–726.
[27] M.R. Wang, X.D. Shan, N. Yang, Phys. Lett. A 376 (2012) 3514–3517.
[28] M.R. Wang, N. Yang, Z.Y. Guo, J. Appl. Phys. 110 (2011) 064310.
[29] D.W. Brenner, O.A. Shenderova, J.A. Harrison, S.J. Stuart, B. Ni, S.B. Sinnott, J. Phys. Condens. Matter 14 (2002) 783–802.
[30] B.W. Dodson, Phys. Rev. B 35 (1987) 2795–2798.
[31] J. Tersoff, Phys. Rev. Lett. 61 (1988) 2879–2882.
[32] P. Hunenberger, Adv. Polym. Sci. 173 (2005) 105–147.
[33] J.N. Hu, Y. Wang, A. Vallabhaneni, X.L. Ruan, Y.P. Chen, Appl. Phys. Lett. 99 (2011) 113101.
[34] B.W. Li, L. Wang, G. Casati, Appl. Phys. Lett. 88 (2006) 143501.
[35] E. Pereira, Phys. Rev. E 82 (2010) 040101.
[36] N. Yang, N. Li, L. Wang, B. Li, Phys. Rev. B 76 (2007) 020301.
[37] D.H. He, S. Buyukdagli, B. Hu, Phys. Rev. B 80 (2009) 104302.
[38] G. Eda, G. Fanchini, M. Chhowalla, Nat. Nanotechnol. 3 (2008) 270–274.
[39] R.S. Pantelic, J.W. Suk, C.W. Magnuson, J.C. Meyer, P. Wachsmuth, U. Kaiser, R.S. Ruoff, H. Stahlberg, J. Struct. Biol. 174 (2011) 234–238.
[40] J.Q. Broughton, G.H. Gilmer, J. Chem. Phys. 79 (1983) 5095–5104.
[41] D.K. Christen, G.L. Pollack, Phys. Rev. B 12 (1975) 3380–3391.
[42] H. Kaburaki, J. Li, S. Yip, H. Kimizuka, J. Appl. Phys. 102 (2007) 043514.
[43] K.V. Tretiakov, S. Scandolo, J. Chem. Phys. 120 (2004) 3765–3769.
[44] I.J. Gupta, S.K. Trikha, Phys. Status Solidi B 84 (1977) K95–K99.
[45] G.K. White, S.B. Woods, Nature 177 (1956) 851–852.
[46] Z.R. Zhong, X.W. Wang, J. Xu, Numer. Heat Transf., Part B, Fundam. 46 (2004) 429–446.
[47] J. Shiomi, S. Maruyama, Phys. Rev. B 73 (2006) 205420.
[48] A.J.C. Ladd, B. Moran, W.G. Hoover, Phys. Rev. B 34 (1986) 5058–5064.
[49] A.J.H. McGaughey, M. Kaviany, Phys. Rev. B 69 (2004) 094303.
[50] J.E. Turney, E.S. Landry, A.J.H. McGaughey, C.H. Amon, Phys. Rev. B 79 (2009) 064301.
[51] A.S. Henry, G. Chen, J. Comput. Theor. Nanosci. 5 (2008) 141–152.
[52] N. de Koker, Phys. Rev. Lett. 103 (2009) 125902.
[53] B. Qiu, H. Bao, G.Q. Zhang, Y. Wu, X.L. Ruan, Compos. Mater. Sci. 53 (2012) 278–285.
[54] L. Wirtz, A. Rubio, Solid State Commun. 131 (2004) 141–152.
[55] B. Qiu, X.L. Ruan, Appl. Phys. Lett. 100 (2012) 233105.